EGM Reconstruction from BSPs in Atrial Fibrillation Using Deep Learning

Miriam Gutiérrez-Fernández[a], Miguel Ángel Cámara-Vázquez[a], Ismael Hernández-Romero[b], Carlos Fambuena-Santos[b], María S Guillem[b], Andreu M Climent[b], Óscar Barquero-Pérez[a]

[a] Universidad Rey Juan Carlos, Fuenlabrada, Madrid, Spain
[b] ITACA Institute, Universitat Politècnica de València, València, Spain

Abstract

Cardiac mapping is a technique for diagnosing and treating arrhythmias by characterizing the electrical activity of the heart. Electrocardiographic Imaging (ECGI) uses electrodes on the torso to capture Body Surface Potentials (BSPs) to reconstruct electrical potentials and repolarization patterns from the surface of the heart non-invasively. Current ECGI algorithms, however, lack noise robustness and stability. This paper proposes a method to reconstruct the electrical activity of the heart using a combination of two architectures: a convolutional autoencoder to extract features from BSPs and a CNN-LSTM Network to reconstruct the electrograms (EGMs) from the extracted features. The proposed strategy was evaluated on 44 atrial fibrillation computational models and provided maximum mean values of correlation of 0.5 and minimum mean RMSE values of 0.48. The reconstruction, latent space and real EGMs maintain the same spectral information, yielding a promising method to address this problem.

1. Introduction

Cardiac mapping aims to represent and characterize the heart's electrical activity and involves recording action potentials in an invasive (intracardiac electrogram) or non-invasive way. Mapping the heart's activity provides clinicians with key information to ablate the arrhythmia source [1]. This is particularly valuable in diagnosing and treating Atrial Fibrillation (AF), known as the most prevalent sustained cardiac rhythm disorder, whose substrate location and electrical dynamics remain unknown [2].

The current method for cardiac mapping involves an invasive and time-consuming technique of placing an array of catheters directly over the heart tissue to perform mapping and ablation [1]. However, this technique has significant limitations, such as providing non-global and asynchronous recordings and offering limited spatial knowledge due to the substantial distance between catheter sensors and the complex atrial anatomy. Aware of these limitations, researchers have put in a lot of effort to develop non-invasive techniques in recent years to overcome these issues. One promising approach involves placing electrodes on the surface of the torso together with CT scans to reconstruct epicardial potentials, known as Electrocardiographic Imaging. This technique provides valuable diagnostic information while minimizing the risks and drawbacks associated with invasive catheter mapping [3].

In this context, Electrocardiographic Imaging (ECGI) methods typically use a vest with 250 electrodes on the torso to capture Body Surface Potentials (BSPs), which combined with geometrical data from a CT or MRI scans, enable the reconstruction of the electrical potentials and repolarization patterns from the surface of the heart [4]. Nonetheless, current approaches fail to yield noise robustness and stability in results, partially due to the ill-posed nature of the inverse problem in electrocardiography [5].

Deep Learning-enabled applications have multiplied in the last years due to the powerful potential to solve very complex tasks that are unreachable with traditional methods. In the case of reconstructing cardiac activity, multiple works have been published addressing this problem by means of deep neural networks. In [6], transfer learning and deep neural networks are used to identify post-infarct ventricular tachycardia (VT) ablation targets. Similarly, in [7] a CNN Convolutional Neural Network (CNN) architecture based on ResNeXt-50 is utilized to estimate the coordinates of VT drivers. Other promising approaches include physical or physiological information apart from the BPMs signals to generate the electrograms (EGMs) signals, such as in [8] or [9].

In this work, we propose a method that aims to reconstruct the electrical activity from BSPs by combining two architectures: a convolutional autoencoder to extract features from BSPs and a CNN-LSTM (Long Short-Term Memory) Network to reconstruct the EGMs from the extracted features. Electrophysiologists' performance could benefit from developing robust and non-invasive techniques, contributing to safer and faster interventions in patients with AF. Deep learning-enabled tools represent a promising approach to tackling this problem on account of their proven capacity to accomplish similar clinical chal-

lenges. The key advantage lies in its adaptability and its ability to capture non-linear relationships in data.

2. Methods

2.1. Computerized models

EGMs were generated using two realistic computerized models of the atria (N=2039 nodes), with the atrial tissue represented by a simplified endocardium-epicardium layer, as previously done in [10], [11]. The forward problem is then computed to obtain the BSPs, using ten torso models (M=659 nodes). The resulting BSPs consist of 440 signals generated using different complexity propagation schemes and driver locations, sampled at $fs = 500Hz$ with a duration from 2 to 5 seconds [12].

2.2. Autoencoders

Autoencoders are a type of neural network commonly used for unsupervised learning tasks such as dimensionality reduction and feature extraction. They comprise an encoder network, which transforms the input data to a lower-dimensional representation (latent space), and a decoder network, which reconstructs the original input from the latent space. Convolutional autoencoders (CAEs) are autoencoder variants that use convolutional layers to learn spatially organized representations of input data, such as images. CAEs have been employed in a wide range of applications, including image denoising, super-resolution, and anomaly detection [13].

2.3. 3D CNN and LSTM

As mentioned, autoencoders may include convolutional layers to exploit local connectivity in images. Convolutional neural networks (CNN) are often used in computer vision to extract spatial information from input data using convolutional and pooling layers. In 3D dimensional convolutional layers, several filters or kernels are convolved to the input array in the three dimensions (width, length, and depth), resulting in various feature maps. The pooling layer that follows decreases the spatial scale of the convolutional layer output. Because these layers are typically followed by a dense layer, the convolutional network output must first be flattened [13]. The combination of 3D-CNN and LSTM architectures enables feature extraction from the sequence of frames (CNN) followed by layers that exploit temporal correlations and keep a "memory" between frames (LSTM).

The proposed architecture comprises two different networks. The former consists of a CAE of 3D convolutional layers and pooling/upsampling symmetrical layers, which aims to extract fundamental information from BSPs. In the second network, the obtained latent space is passed through 3D convolutions and upsampling layers, LSTM layers and a final dense layer to reconstruct the original EGM signals. The chosen activation function is Leaky ReLU to avoid dying ReLU and exploding or vanishing gradients. Several methods of regularization are employed, such as early stopping, batch normalization, dropout and L2 penalization in the loss function (MSE error).

2.4. Performance Metrics

To assess the quality of the models, the following metrics are used, which are utilized to evaluate two different signals depending on the network: in the CAE network, BSPs and reconstructed BSPs are evaluated. On the other hand, in the reconstruction network, the reconstructed EGMs are assessed.

- Mean Squared Error (MSE): Which is used as the loss function

$$MSE = \frac{1}{N}\sum_{i=1}^{N}(\hat{y} - y)^2 \tag{1}$$

where N is the number of samples in a batch, $\hat{y}$ is the reconstructed signal and y is the real signal.

- Mean Absolute Error (MAE)

$$MAE = \frac{1}{N}\sum_{i=1}^{N}|\hat{y} - y| \tag{2}$$

where N is the number of samples in a batch, $\hat{y}$ is the reconstructed signal and y is the real signal.

- Spearman Correlation (SC): SC correlation coefficient is a statistical measure of the strength of the relationship between two variables,

$$\rho = 1 - \frac{6\sum d_i^2}{n(n^2-1)} \tag{3}$$

where ρ is the SC coefficient that ranges from -1 to 1, d is the difference in the rankings of each observation in the two samples under consideration, and n is the number of observations in each sample.

- Root Mean Squared Error (RMSE), can be defined as:

$$\sqrt{MSE} \tag{4}$$

2.5. Experimental setup

The final raw dataset of BSPs is comprised of 440 BSP models of 64 nodes and 44 EGM models with 512 nodes. Following, the signals are preprocessed to adequate them for training the models. First, gaussian noise is added to 20 dB, followed by a filtering step using a Butterworth pass band filter between 3 and 30 Hz. Then, the signals are downsampled to 50 Hz to avoid redundant batches during the training of LSTM layers. Next, the 64 flat nodes are set in a rectangular array, hence producing 6 x 12 images, resembling an unfolded cylinder scheme. Subsequently, the

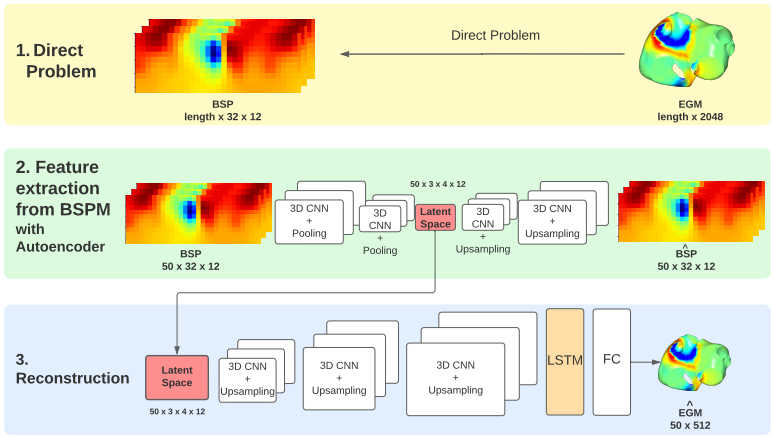

Figure 1. Diagram of the architecture used to process one single AF Model of length 3000 samples. The process is defined by 1) Direct problem, 2) feature extraction from BSPs with an autoencoder and 3) reconstruction.

image size is increased to 12 x 24 using bilinear interpolation. Finally, BSPs are divided into train, test and validation subsets ensuring that BSPs coming from the same AF models are included in the same subset, therefore avoiding the leaking of information from train to test.

The latent space obtained from the autoencoder and the real EGMs, which are used as the input and output for the reconstruction network respectively, are normalized between -1 and 1 and centered. For the regression network, each BSPs model is assigned as ground truth the original AF Model from which it was generated. In behalf of a reduction in the complexity of the models, the number of nodes is reduced from 2048 to 512 evenly.

3. Results

The general results for the autoencoder show a MSE of 0.002 and a mean MSE of 0.024 over all the AF Models. Good results and metrics are obtained from the feature extraction, as almost a perfect recovery of the input BSPs is obtained. The resulting latent space in time is difficult to interpret under simple eye inspection, as it is the result of several layers of convolution and pooling. On the other hand, the reconstruction network produces an overall MSE of 0.175 and MAE of 0.32. Performance is computed as well separately for each of the 9 randomly selected AF models that conform the test subset. The results obtained for the SC coefficient show that the mean correlation among the 512 nodes reaches 0.5 in some models, achieving values around 0.75 in some nodes. However, these results are not fully consistent in every test model, as depicted in Figures 2. The mean RMSE results show something similar, providing a minimum value of 0.47 as shown in Figure 2. In Figure 3, four randomly selected realizations of the test subset are presented, yielding similar frequency correlation, although morphology similarity is still questioned. The Welch periodogram, represented in Figure 4, was computed for the original EGM signals, the produced latent space and the reconstructed EGM signals, using a sliding window of size 200 samples. The results show that the spectral activity in the 3 cases is rather similar, confirming that the periodic patterns of AF are kept during the feature extraction and later reconstruction.

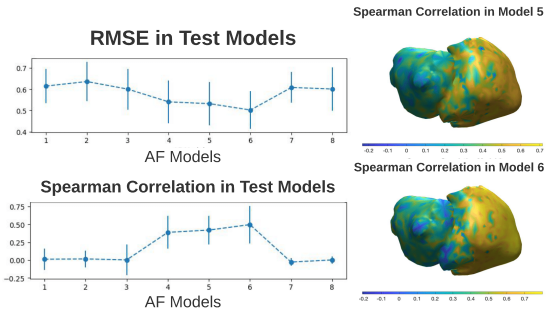

Figure 2. Mean and standard deviation of SC and RMSE of the 512 nodes among the 9 test models (left) and correlation maps in two random test AF models (right)

4. Conclusions and discussion

The proposed architecture showed significant potential for accurately reconstructing EGMs in complex signals like AF. In some cases, it was able to reproduce high-frequency content without the need for a transfer matrix, which is typically required in classical approaches based on inverse-problem solutions. These findings suggest that the proposed architecture may offer an alternative solution for ECGI apart from to traditional methods. However, further research is necessary to evaluate its performance on

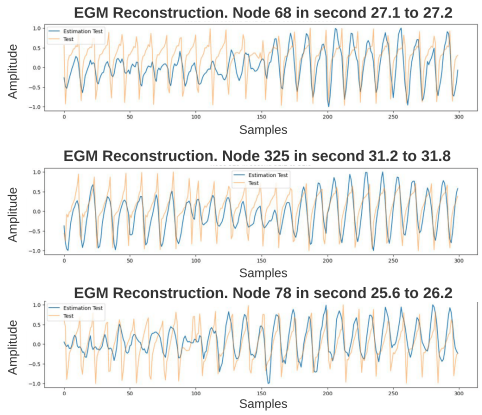

Figure 3. Random reconstructions, in orange, the original EGMs and in blue, the reconstructed signal.

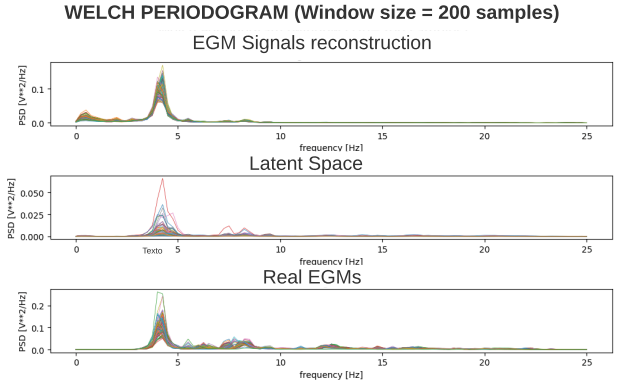

Figure 4. Welch periodogram for the reconstructed EGMs, the produced latent space and the original EGM signals

larger datasets and in different clinical scenarios. The next steps would require a deeper assessment of the architecture regarding data handling and arrangement. Further modifications of the architecture include a parameter of regularization to penalize the autoencoder's loss function if the reconstructions are not satisfactory.

Acknowledgments

This work has been partially supported by: Ministerio de Ciencia (PID2019-105032GB-I00, PID2022-136887NB-I00), Universidad Rey Juan Carlos (2023/00004/006-F918), Instituto de Salud Carlos III, and Ministerio de Ciencia, Innovación y Universidades (supported by FEDER Fondo Europeo de Desarrollo Regional PI17/01106 and RYC2018-024346B-750), Consejería de Ciencia, Universidades e Innovación of the Comunidad de Madrid through the program RIS3 (S-2020/L2-622), EIT Health (Activity code 19600, EIT Health is supported by EIT, a body of the European Union) and the European Union's Horizon 2020 under the Marie Skłodowska-Curie grant agreement No. 860974.

References

[1] Shenasa, et al. "Cardiac mapping". John Wiley & Sons, 2019.

[2] Hindricks G, et al. "2020 ESC Guidelines for the diagnosis and management of atrial fibrillation developed in collaboration with the european association for Cardio-Thoracic Surgery". European heart journal 2021;373–498.

[3] Issa ZF, et al. "Advanced Mapping and Navigation Modalities". In Issa ZF, Miller JM, Zipes DP (eds.), Clinical Arrhythmology and Electrophysiology: A Companion to Braunwald's Heart Disease (Second Edition). W.B. Saunders, 2012; .

[4] Hernández-Romero I, et al. "Electrocardiographic imaging in the atria". Medical Biological Engineering Computing 2022;1–18.

[5] Rodrigo M, et al. "Body surface localization of left and right atrial high-frequency rotors in atrial fibrillation patients: A clinical-computational study". Heart Rhythm 2014;11:1584–1591.

[6] Monaci S, et al. "Non-invasive localization of post-infarct ventricular tachycardia exit sites to guide ablation planning: a computational deep learning platform utilizing the 12-lead electrocardiogram and intracardiac electrograms from implanted devices". Europace 2023;469–477.

[7] Pilia N, et al. "Non-invasive localization of the ventricular excitation origin without patient-specific geometries using deep learning". Artificial Intelligence in Medicine 2022;.

[8] Bacoyannis ea. "Deep learning formulation of ECGI evaluated on clinical data". Europace 2022;24(Supplement_1).

[9] Tenderini ea. "PDE-aware deep learning for inverse problems in cardiac electrophysiology". SIAM Journal on Scientific Computing 2022;44(3):B605–B639.

[10] Gutierrez-Fernández M, Cámara-Vázquez Má, Hernández-Romero I, Guillem MS, Climent AM, Barquero-Pérez Ó. "Non-Invasive Atrial Fibrillation Driver Localization Using Recurrent Neural Networks and Body Surface Potentials". In 2022 Computing in Cardiology (CinC). 2022; .

[11] Cámara-Vázquez M, et al. "Non-invasive estimation of atrial fibrillation driver position with convolutional neural networks and body surface potentials". Frontiers in Physiology 2021;.

[12] Rodrigo M, et al. "Technical considerations on phase mapping for identification of atrial reentrant activity in direct- and inverse-computed electrograms". Circulation Arrhythmia and Electrophysiology 2017;.

[13] Goodfellow I, Bengio Y, Courville A. Deep learning. MIT press, 2016.

Address for correspondence:

Miriam Gutiérrez Fernández-Calvillo miriam.gutierrez@urjc.es
Rey Juan Carlos University, Cam. del Molino, 5, Madrid, 28942, Spain